Surface Science 604 (2010) 1889–1893

Contents lists available at ScienceDirect

Surface Science

journal homepage: www.elsevier.com/ locate/susc

Adsorption of atomic oxygen on cubic $PbTiO_3$ and $LaMnO_3$ (001) surfaces: A density functional theory study

G. Pilania *, R. Ramprasad

Chemical, Materials, and Biomolecular Engineering, Institute of Materials Science University of Connecticut, Storrs, CT 06269, United States

ARTICLE INFO

Article history:
Received 24 May 2010
Accepted 22 July 2010
Available online 6 August 2010

Keywords:
Perovskites
Oxygen adsorption
Density functional theory

ABSTRACT

We present and discuss density functional theory calculations addressing the electronic structure and energetics of isolated oxygen ad-atoms at the (001) surfaces of $PbTiO_3$ (PTO) and $LaMnO_3$ (LMO) cubic perovskites. Both AO- and BO_2-type of surface terminations are considered for each perovskite. Difference electron density analysis has been carried out for each surface to probe local electronic charge redistribution upon oxygen adsorption. Our results show that the (001) surfaces of the two perovskites behave quite differently towards oxygen adsorption. In the case of the PTO (001) surfaces, the adsorbate oxygen atom was found to form a peroxide-type molecular species along with a surface lattice oxygen atom on both PbO- and TiO_2-terminated surface facets. On the other hand, the most stable oxygen adsorption site for the LMO (001) surfaces corresponds to the one expected from a natural continuation of the perovskite lattice. Moreover, the dissociative adsorption of molecular oxygen varies from being only slightly exothermic on the PTO (001) facets to being highly exothermic on the LMO (001) facets. The AO-terminated facets, in general, showed a stronger binding to the adsorbed oxygen.

1. Introduction

Apart from their importance in many technological applications such as sensors and photocatalysis, perovskite oxides (with the generic chemical formula given as ABO_3) have received considerable attention as high temperature oxygen ion and proton conductors for their use in solid oxide fuel cells (SOFC) and electrochemical applications [1-5]. Recently, they have also been reported to bear catalytic properties superior to the conventional Pt-based catalysts for the deNO_x process (*i.e.* removal of NO_x gases) in catalytic convertors of auto exhausts [6,7]. The underlying processes in both such applications involve interaction of the perovskite surface with the gas phase oxygen. Therefore, acquiring a fundamental understanding of the nature of the interaction between oxygen and the perovskite surfaces is crucial to explain the role of oxygen in such technological processes.

The ability of a perovskite surface to undergo reversible oxygen chemisorption represents a key feature of its catalytic activity towards any oxidation reactions and is usually associated with the mixed valence states of the transition metal ion B. One may expect such an oxidation reaction to proceed through several elementary steps each involving either oxygen vacancies or ad-atoms or both. However, many reports in the literature suggest that the formation of an oxygen vacancy in a pure ABO_3 perovskite is a highly endothermic process [8-13] and therefore only a very low concentration of equilibrium oxygen vacancies is expected even at high temperatures in a pure ABO_3 perovskite (we however note that significant oxygen vacancy concentration can be achieved even at lower temperatures by chemical doping at the A or B cation sites with a metal ion having a lower oxidation state [14-16]). Moreover, molecular oxygen has a strong tendency for getting adsorbed on a surface vacancy site and thereby annihilating it and forming a surface adsorbed O ad-atom. A second route for the formation of O ad-atom is provided through the dissociative adsorption of O_2 on the oxide surface. Therefore, it has been postulated that the atomic form of oxygen adsorbed on the surface is the active species in the case of a higher temperature intrafacial catalysis [17].

A necessary prerequisite for the atomic scale understanding of oxygen dynamics on a perovskite surface is the knowledge of the electronic structure and the local environment of the active sites on the surface. The difficulties associated with distinguishing between surface adsorbed and lattice oxygen have significantly limited interpretation of available experimental data. Furthermore, experimental studies to date are still unable to identify the active sites for the oxygen reduction reaction at the perovskite surfaces. Density functional theory (DFT) calculations may be a powerful approach to elucidate the oxygen–surface interactions and can provide details about the electronic structure, geometrical parameters, and energetics of the bulk and adsorbed intermediate species.

Despite the broad technological implications, first principles studies aimed at modeling oxygen adsorption on perovskite surfaces are very scarce in the literature. Recently, density functional theory (DFT) calculations by Piskunov et al. [18] and Guhl et al. [19]

* Corresponding author.
E-mail addresses: gpilania@gmail.com (G. Pilania), rampi@ims.uconn.edu (R. Ramprasad).

0039-6028/$ – see front matter © 2010 Elsevier B.V. All rights reserved.
doi:10.1016/j.susc.2010.07.021

confirmed the formation of molecular peroxide (O_2^{-2}) species suggested by experimental spectroscopic and kinetic investigations [20,21] on both of the regular terminations of $SrTiO_3$ (001) surfaces. A detailed DFT study exploring mechanisms of oxygen reduction on highly polar (110) surfaces of cubic $LaMnO_3$ (LMO) was reported by Choi et al. [22] showing that the oxygen dissociation occurs with small reaction barriers or without any barrier at both perfect and defective LMO surfaces and involves superoxo- or peroxo-like intermediate species. Another DFT study by Kotomin et al. [23] for the low temperature orthorhombic LMO (001) surface facets demonstrated that the dissociative adsorption of O_2 molecules from the gas phase is energetically favorable on the Mn surface ions even on a defect-free surface.

Here we report periodic DFT calculations aimed at a study of the energetics and local electronic structure of oxygen adsorption on the (001) surfaces of $PbTiO_3$ (PTO) and LMO. The choice of PTO and LMO as model systems is motivated by the fact that these are intrinsically different in terms of the oxidation states displayed by their A (Pb^{+2} and La^{+3}) and B (Ti^{+4} and Mn^{+3}) site cations. Furthermore, the (001) facets in PTO (terminated by either the PbO or TiO_2 layers) are non-polar while the LMO (001) facets (terminated by either the LaO or MnO_2 layers with nominal charges ± 1 e per layer in a (1×1) supercell) represent polar surfaces. Moreover, unlike Ti in PTO, Mn in LMO is more flexible towards supporting variable oxidation states.

Also, keeping in mind the associated high operating temperatures in applications such as SOFC and catalytic convertors in auto-exhausts, the high temperature cubic perovskite phase is considered in the present study. Thus, even though the first principles calculations presented here are performed at 0 K, the fixed cubic symmetry can provide useful results for the high temperature cubic phase of both PTO and LMO.

2. Computational and model details

DFT calculations were performed with the periodic supercell plane-wave basis approach implemented in the Vienna *Ab initio* Simulation Package (VASP) [24]. The interactions between the valence and the frozen core electrons were simulated with the projector augmented wave (PAW) method, [26] and electron exchange and correlation were treated within the local density approximation (LDA) [25]. In keeping with a large number of prior studies of PTO using the LDA, [27-32] we continue with this approximation in the present work as well. Tests using the generalized gradient approximation (GGA) instead of LDA, however did not yield any qualitative differences with respect to the conclusions concerning O chemistry that arrived at in the present study. Plane waves were included to a cutoff of 500 eV and the O 2s and 2p, the Ti 3s, 3p, 3d and 4s, the Mn 3p, 4s and 3d, the Pb 5d, 6s, and 6p, La 5s, 5p, 5d and 6s electrons were included in the valence states. Spin-polarized calculations were adopted to properly describe magnetism inherent to LMO based systems (bulk and surfaces) and the triplet ground state of oxygen molecule. A Monkhorst-Pack *k-point* mesh [33] of $8\times8\times8$ yielded well converged bulk results.

Within these approximations the calculated PTO and LMO bulk lattice constants in the cubic phase are predicted to be 3.887 Å and 3.802 Å, respectively, underestimated with respect to their corresponding experimental values of 3.97 Å [34] and 3.947 Å [35]. These calculated bulk lattice constants were then further used to construct surface models in the form of slab geometries. The PTO and LMO (001) surfaces both in the absence and the presence of O ad-atoms were modeled using symmetric slabs (with respect to the central mirror plane) consisting of nine alternating AO and BO_2 layers. Geometry optimization of all slabs (both in the absence and the presence of O ad-atoms) was accomplished by requiring the forces experienced by each atom to be smaller than 0.04 eV/Å. A vacuum of approximately 12 Å was placed above the slabs in order to avoid any spurious interaction between adjacent slabs along the slab surface normals. The average surface energy of AO- and BO_2-terminated clean (001) surfaces fluctuated within 0.1 meV/Å^2 going from nine layers to eleven layers for both the PTO and LMO.

To model surface oxygen adsorption, O ad-atoms were placed symmetrically on both sides of the slab, thus preventing the possibility of any non zero dipole moment perpendicular to the surface. For each of the AO- and BO_2-terminated surfaces, five different adsorption sites for O ad-atoms were considered. These are shown schematically in Fig. 1. In each case, a (2×2) supercell was used to model a dilute-limit coverage of O ad-atoms on the surface of interest. A Monkhorst-Pack *k-point* mesh of $4\times4\times1$ was employed to produce converged results for all such slabs.

The oxygen ad-atom binding energy with respect to a free oxygen molecule in the gas phase is defined as

$$E_b = \frac{1}{2}\left[E_{surf-O_{ad}} - E_{surf} - E_{O_2}(gas)\right] \quad (1)$$

where $E_{surf\text{-}O_{ad}}$, E_{surf} and E_{O_2} (gas) represent the total energy of the relaxed adsorbate covered surface system, the total energy of the clean surface and the total energy of an O_2 molecule in the gas phase, respectively. A negative value of E_b indicates that the dissociative adsorption of the O_2 molecule is exothermic on the surface. A factor of 2 in the denominator arises from the fact that the O_{ad} is adsorbed symmetrically on both sides of the slab. The binding energy thus obtained using the above equation is referenced to a gas phase O_2 molecule in its spin-triplet ground state.

3. Results and discussion

3.1. PTO surfaces

The most stable geometric structure produced due to the oxygen adsorption on each of the four different surfaces considered here is shown in Fig. 2. In the case of the PTO (001) surfaces, for both PbO- and TiO_2-terminations, the adsorbate binds to a surface lattice oxygen atom forming a peroxide-type (O_2^{-2}) molecular species. Recently similar phenomenon has also been reported for the $SrTiO_3$ (001) surfaces [18,19]. On the PbO-termination PTO (001) surface, the oxygen ad-atom (O_{ad}) is adsorbed exothermically on a Pb–O bridge site with a binding energy $E_b = -0.89$ eV. The directly coordinated lattice oxygen is pulled out of the surface while the underlying Ti atom is pressed into the bulk, thereby stretching the Ti–O bond from 1.945 Å to 2.09 Å. The bond length between the O_{ad} and the lattice oxygen was found to be 1.45 Å which is quite close to the O–O bond length in the H_2O_2 molecule and is a characteristic of molecular peroxide species [36]. The distance between the O_{ad} and the nearest surface Pb atom is 2.26 Å and the surface O_{ad}–O bond is tilted with respect to the surface normal with an O_{ad}–O–Ti angle of 124° (*c.f.* Fig. 2a).

Although the Pb–O bridge site is the most energetically favored site, the resulting configuration due to the O_{ad} adsorption at the 3-fold site, being only 0.09 eV higher in energy, is almost equally energetically favored and can simply be obtained by a 45° rotation of the dioxygen complex around the surface normal. The O_{ad}–O bond length and O_{ad}–O–Ti bond angle in this configuration are essentially the same as those mentioned above for the Pb–O bridge site adsorption. Therefore,the tilt direction of the dioxygen moiety on the PbO-terminated (001) surface, with a negligible barrier towards a 90° rotation around the surface normal, is expected to exhibit some dynamics at high temperatures.

At the TiO_2-terminated surface, the O_{ad} binds exothermically at the Ti–O bridge site. However, the binding is weaker by 0.36 eV than on the more ionic PbO-terminated surface. The relaxed geometry for the adsorbate system is shown in Fig. 2b. The O_{ad}–O bond length is 1.43 Å,

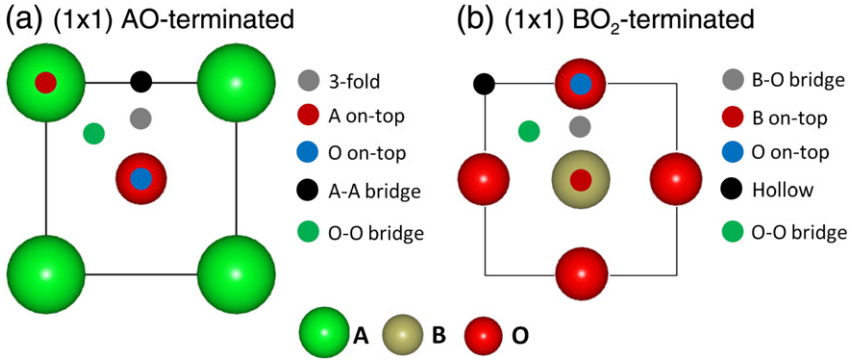

Fig. 1. Schematic top view of five possible adsorption sites considered in the present study on (a) AO- and (b) BO_2-terminated (001) surfaces.

again falling in the range expected for the molecular peroxide species. Showing a similar behavior to the PbO-terminated surface, the O_{ad} on this surface binds close to the lattice O and is tilted towards one of the adjacent surface Ti atom such that the Ti–O_{ad}–O and O–Ti–O_{ad} angles and the Ti–O_{ad} bond length are 74.8°, 42.5° and 1.88 Å, respectively. Despite the Ti–O bridge site being the most energetically preferred adsorption site, the O-ontop adsorption site is only 0.39 eV higher in energy and serves as a saddle point for a flipping motion of the dioxygen moiety towards the other neighboring surface Ti atom. The computed barrier (0.39 eV) for the flipping motion compares well with that reported for the TiO_2-terminated surface of $SrTiO_3$ (0.30 eV) [19].

To visualize the charge rearrangements upon the O_{ad}-surface bond formation, we further carried out the difference electron density [37] analysis presented in Fig. 3. The difference electron density is obtained by subtracting the electron charge density of both an isolated O atom and a clean surface from that of the relaxed surface with an O adatom. To highlight only the local rearrangements in the electronic charge density occurring due to the O_{ad}-surface bonding, the atomic positions of the clean surface and the O_{ad} are taken to be same as those of the relaxed adsorbate-surface system.

The analysis of the electron density redistribution due to the O_{ad} adsorption for the PbO- and TiO_2-terminated (001) surfaces is shown in Fig. 3a and b, respectively, which further confirms the formation of a quasi-molecular species between O_{ad} and a directly coordinated lattice O atom. We note that the O_{ad} bonding induced electronic charge redistribution on both of the (001) facets of PTO is quite locally confined in the vicinity of O_2^{-2} molecular species and the charges on all other atoms remain virtually unaffected due to the bonding. A clear donation of charge from the lattice O to the O_{ad} is visible. Bader charge analysis [38,39] further shows that the charge surplus at the lattice oxygen is somewhat evenly distributed between the O atoms forming the peroxide-like O–O_{ad} moiety (0.82 e and 0.94 e on PbO-terminated and 0.75 e and 0.52 e on TiO_2-terminated surfaces, respectively) after adsorption.

The suggested formation of the O_2^{-2} molecular species on the PTO (001) surfaces is further supported by an analysis of the local density of states obtained by projecting the total density of states (DOS) of the relaxed adsorbate-surface system on to the surface $O_{lattice}$–O_{ad} moiety for both PbO- and TiO_2-terminated surfaces (*c.f.* Fig. 4a and b,

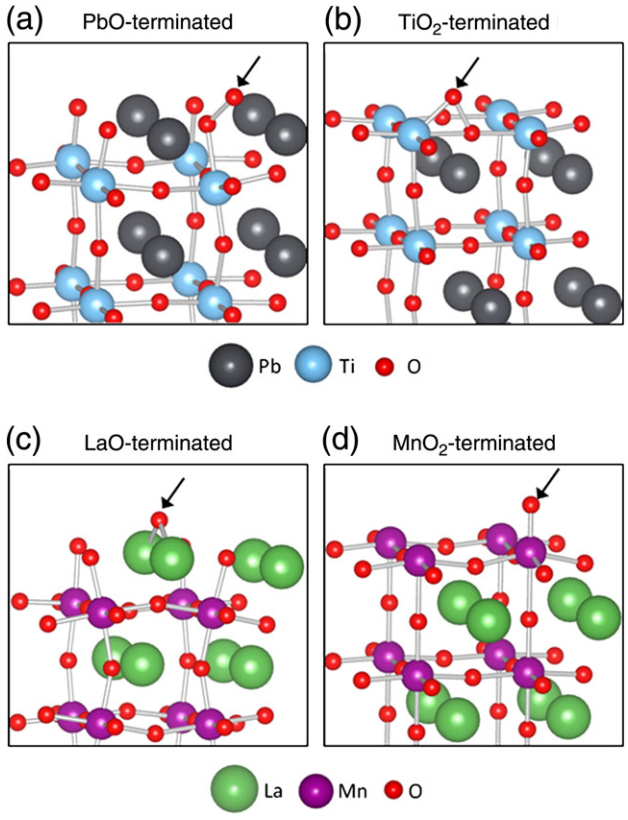

Fig. 2. The most stable O adsorption geometries on the PbO-terminated (a) and TiO_2-terminated (b) facets of PTO, and on the LaO-terminated (c) and MnO_2-terminated (d) facets of LMO. The O_{ad} is indicated by an arrow in each of the four panels.

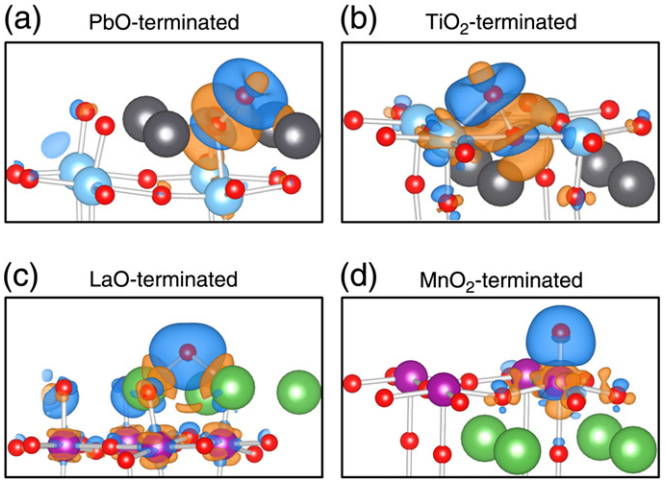

Fig. 3. Difference electron density maps highlighting the electron charge density redistribution due to the O_{ad} adsorption for the (a) PbO-, (b) TiO_2-, (c) LaO- and (d) MnO_2-terminated (001) cubic perovskite surfaces. An isosurface corresponding to an electron charge density of 0.02 e/Å^3 is shown in each of the panels. Red and blue colors have been used to represent depletion and accumulation of charge, respectively. The representation of atoms is same as that used in Fig. 1.

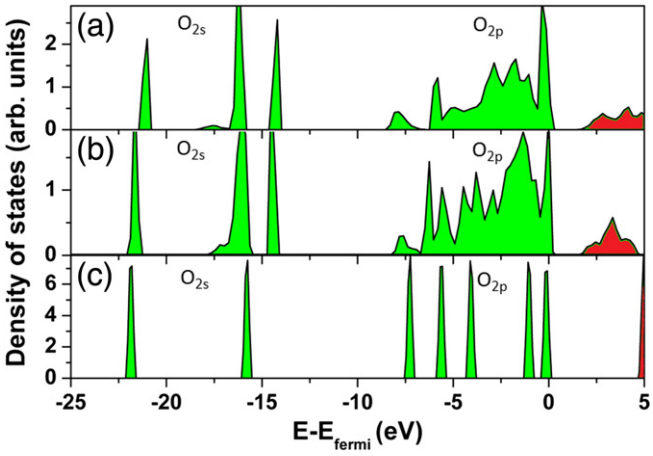

Fig. 4. Density of states analysis supporting the formation of O–O_{ad} peroxide moiety at PbO- and TiO_2-terminated surfaces. The top two panels show the DOS projected onto the 2s and 2p states of O_{ad} and the directly coordinated lattice O for PbO- (a) and TiO_2-termination (b), identifying two sharp states above and below the O 2s group as fingerprints of the formed peroxide moiety. The same O projected DOS of an H_2O_2 molecule exhibiting essentially the same characteristic is shown in panel (c). The occupied and unoccupied levels are shaded green and red, respectively.

respectively). The corresponding local DOS when compared with the oxygen projected DOS of an H_2O_2 molecule (Fig. 4c), in which O_2^{-2} species occurs naturally, shows clear fingerprints of a peroxide-like dioxygen moiety formation at each of the surface.

3.2. LMO surfaces

Unlike the non-polar regular terminations of PTO (001) facets, an LMO (001) surface may display one of the two terminations of opposite polarity with effective charges of +1 e (LaO-terminated) or −1 e (MnO_2 terminated), respectively, owing to the nominal charge states of +3, +3 and −2, respectively, for La, Mn and O in LMO. We also note that while the top of the valance band in PTO is mainly generated by oxygen 2p states, [40] f-states of La and d states of Mn (with only a small contribution from oxygen 2p states) contribute largely to the formation of electronic bands near the fermi level in LMO (which is a metal unlike PTO) [41]. Owing to the distinctly different oxidation states of the transition metals in the case of LMO (relative to PTO), the consequent polarity (and unsaturations) of the LMO surfaces, and the underlying electronic structure, the most preferred oxygen adsorption sites on LMO (001) surfaces are expected to be those simply dictated by the natural extension of the perovskite lattice, in contrast to that on PTO (001) surfaces.

Our findings for the optimal geometries for O adsorbed LMO surfaces are consistent with the above expectations. The LaO-terminated surface adsorption of the O_{ad} atom at the La–La bridge site results in the most energetically favorable configurations with a La–O bond length of 2.15 Å, much shorter than the bulk La–O bond length of 2.69 Å. As a result of O_{ad} atom adsorption, a significant surface relaxation takes place on the surface through tilting of the neighboring MnO_2 octahedra away from the O_{ad} atom around an axis parallel to the [010] direction (*c.f.* Fig. 2c) with a tilt angle of 11.5°. Unlike the PTO (001) surfaces discussed above, where the charge redistribution due to the O_{ad} atom binding on the surface is quite confined to regions close to the adsorbate, the O_{ad} atom approaching to the LMO surface can be described as an oxygen ion carrying two holes which tend to delocalize by hopping down the surface giving rise to a strong bond.

This view point is further strengthened by the difference electron density plot in Fig. 3c, where a significant charge redistribution in the penultimate MnO_2 layer is clearly evident after O_{ad} atom binds at the topmost LaO surface layer. A combined effect of the adsorption induced surface relaxations through MnO_2 octahedra tilting as well as the stabilization through a long range charge delocalization gives rise to a highly exothermic binding energy of $E_b = -4.57$ eV on this surface. This large exothermicity may also be understood in terms of the coordinative unsaturation prevalent at the LaO-terminated surface (as this surface may be viewed as sub-stoichiometric with respect to the parent oxide of La, namely, La_2O_3).

The MnO_2-terminated surface shows a strong preference for O_{ad} adsorption over the surface Mn ion with a Mn–O_{ad} bond length of 1.60 Å. As shown in Fig. 2d, due to the surface bond formation the Mn ion is pulled out of the surface, resulting in a significant stretching of its bond with the O lying in the second topmost layer (with a Mn–O bond length of 2.25 Å as compared to that of 2.02 Å for a clean surface in the absence of O_{ad}). The oxygen binding energy E_b is calculated to be –1.75 eV. Our results are qualitatively similar to those reported for the MnO_2-terminated surface of the low temperature orthorhombic phase of LMO, with a Mn–O_{ad} bond length of 1.63 Å and E_b of −1.07 eV [23]. The Bader charge analysis reveals that a total of 0.63 e charge is transferred to the adsorbed O_{ad}, 0.17 e of which comes from the directly coordinated Mn ion and 0.28 e is contributed by the four nearest O ions on the surface. This is also readily evident from the difference electron density plot in Fig. 3d, where a charge accumulation on the O_{ad} and the corresponding depletion at the surface Mn and four neighboring O ions is clearly depicted as a result of the O_{ad} adsorption on the surface.

4. Conclusions

In conclusion, we have presented a density functional theory study of oxygen adsorption on the (001) facets of cubic PTO and LMO. On both of the regular terminations of the (001) PTO surface, the preferred adsorption site for an O ad-atom is the bridge site between a surface metal ion and surface lattice oxygen. The adsorbed O is found to form a quasi-molecular peroxide-like species with the lattice oxygen. Owing to the stoichiometric charge neutral non-polar nature of these terminations, the charge density redistribution induced by the adsorbed O is found to be quite local, confined in the vicinity of the formed dioxygen moiety. On both the PTO (001) facets the dissociative adsorption O_2 is energetically favored with adsorption at the PbO-terminated facet (−0.89 eV) being slightly more exothermic than that at the TiO_2-terminated facet (−0.53 eV).

In contrast to the PTO (001) surfaces, the most preferred O adsorption sites on the polar LMO (001) surfaces are given by those which would have been naturally occupied by oxygen if we were to further extend the perovskite lattice, *i.e.* the La–La bridge site on the LaO-terminated facets and the Mn-ontop site for the MnO_2-terminated surface. A long range charge delocalization in the penultimate layer, adsorbate induced surface relaxations and most importantly, coordinative unsaturations due to the sub-stoichiometric nature of this surface result in a highly exothermic oxygen binding on the LaO-terminated surface (–4.57 eV). On the MnO_2-terminated surface, charge redistributions are mainly confined to the surface Mn and four neighboring surface O atoms, and O binding is much less exothermic (−1.75 eV).

The drastically different manners of O ad-atom binding (in terms of binding modes, sites and energetics) to the two different perovskite surfaces are a natural consequence of the very different nominal oxidation states of the transition metals involved, and the variation in the electronic structure of the two ABO_3 systems. A detailed understanding of such differences may enable us to optimize the reactivity and possible catalytic activity of such systems.

Acknowledgement

This material is based upon work supported by the Office of Naval Research and the Department of Energy. Partial computational

support through a National Science Foundation Teragrid allocation is also gratefully acknowledged.

References

[1] V.E. Henrich, P.A. Cox, The Surface Science of Metal Oxides, Cambridge Univ. Press, New York, 1994.
[2] C. Noguera, Physics and Chemistry of Oxide Surfaces, Cambridge Univ. Press, New York, 1996.
[3] L.J. Tejuca, J.L.G. Fierro (Eds.), Properties and Applications of Perovskite Type Oxides, Marcel Dekker, New York, 1993.
[4] M.A. Peña, J.L.G. Fierro, Chem. Rev. 101 (2001) 1981.
[5] K. Haung, H.Y. Lee, J.B. Goodenough, J. Electrochem. Soc. 145 (1998) 3220.
[6] Y. Nishihihata, J. Mizuka, T. Akao, H. Talaka, M. Uenishi, M. Kimura, T. Okamoto, H. Hamado, Nature 418 (2002) 164.
[7] C.H. Kim, G. Qi, K. Dahlberg, W. Li, Science 327 (2010) 1624.
[8] Y.F. Zhukovskii, E.A. Kotomin, S. Piskunov, Y.A. Mastrikov, D.E. Ellis, Ferroelectrics 379 (2009) 191.
[9] Y.-L. Lee, D. Morgan, J. Kleis, J. Rossmeisl, ECS Trans. 25 (2009) 2761.
[10] J.H. Kuo, H.U. Anderson, D.M. Sparlin, J. Solid State Chem. 83 (1989) 52.
[11] J. Nowotny, M. Rekas, J. Am. Ceram. Soc. 81 (1998) 67.
[12] J. Mizusaki, M. Yoshihiro, S. Yamauchi, K. Fueki, J. Solid State Chem. 58 (1985) 257.
[13] J. Mizusaki, Y. Mima, S. Yamauchi, K. Fueki, H. Tagawa, Solid State Chem. 80 (1989) 102.
[14] S. Khan, R.J. Oldman, F. Corà, C.R.A. Catlow, S.A. French, S.A. Axon, Phys. Chem. Chem. Phys. 8 (2006) 5207.
[15] M.S.D. Read, M.S. Islam, G. Watson, F. King, F.E. Hancock, J. Mater. Chem. 10 (2000) 2298.
[16] N. Gulhame, M. Primet, Stud. Surf. Sci. Catal. 116 (1998) 581.
[17] R.J.H. Voorhoeve, J.P. Demeika, L.E. Triumble, Ann. N. Y. Acad. Sci. 272 (1976) 3.
[18] S. Piskunov, Y.F. Zhukovskii, E.A. Kotomin, E. Heifets, D.E. Ellis, Proc. Mater. Res. Soc. Symp. 894 (2006) 0894-LL08-05.
[19] H. Guhl, W. Miller, Karsten Reuter, Surf. Sci. 604 (2010) 372.
[20] V.M. Bermudez, V.H. Ritz, Chem. Phys. Lett. 73 (1980) 160.
[21] R. Merkle, J. Maier, Phys. Chem. Chem. Phys. 4 (2002) 4140.
[22] Y. Choi, D.S. Mebane, M.C. Lin, M. Liu, Chem. Mater. 19 (2007) 1690.
[23] E.A. Kotomin, Y.A. Mastrikov, E. Heifets, J. Maier, J. Phys. Chem. Chem. Phys. 10 (2008) 4644.
[24] G. Kresse, J. Furthmüller, Phys. Rev. B 54 (1996) 11169.
[25] R. Martin, Electronic Structure: Basic Theory and Practical Methods, Cambridge University Press, New York, 2004.
[26] P.E. Blöchl, Phys. Rev. B 50 (1994) 17953.
[27] Z. Wu, R.E. Cohen, Phys. Rev. Lett. 95 (2005) 037601.
[28] Z. Wu, R.E. Cohen, D.J. Singh, Phys. Rev. B 70 (2004) 104112.
[29] Y. Duan, H. Shi, L. Qin, J. Phys.: Condens. Matter 20 (2008) 175210.
[30] G. Pilania, S.P. Alpay, R. Ramprasad, Phys. Rev. B 80 (2009) 014113.
[31] T. Shimada, S. Tomoda, T. Kitamura, Phys. Rev. B 79 (2009) 024102.
[32] B. Meyer, D. Vanderbilt, Phys. Rev. B 63 (2001) 205426.
[33] H. Monkhorst, J. Pack, Phys. Rev. B 13 (1976) 5188.
[34] B.G. Shirane, R. Repinsky, Acta Cryst. 9 (1956) 131.
[35] J. Rodrýguez-Carvajal, M. Hennion, F. Moussa, A.H. Moudden, Phys. Rev. B 57 (1998) R3190.
[36] S.A. Kulkarni, L.J. Bartolotti, R.K. Pathak, Chem. Phys. Lett. 372 (2003) 620.
[37] M. Scheffler, C. Stampfl, in: K. Horn, M. Scheffler (Eds.), Handbook of Surface Science, Electronic Structure, vol. 2, Elsevier, Amsterdam, 2000.
[38] R. Bader, Atoms in Molecules: A Quantum Theory, Oxford University Press, New York, 1990.
[39] G. Henkelman, A. Arnaldsson, H. Jónsson, A fast and robust algorithm for Bader decomposition of charge density, Comput. Mater. Sci. 36 (2006) 254.
[40] S. de Lazaro, E. Longo, J.R. Sambrano, A. Beltràn, Surf. Sci. 552 (2004) 149.
[41] D. Fuks, S. Dorfman, J. Felsteiner, L. Bakaleinikov, A. Gordon, E.A. Kotomin, Solid State Ionics 173 (2004) 107.